09,11,03

Nuclear quadrupole interaction of a negatively charged boron vacancy with near and remote nitrogen nuclear magnetic moments in hexagonal boron nitride

© E.V. Dmitrieva[1], G.V. Mamin[1], I.N. Gracheva[1], S.S. Nagalyuk[2], M.R. Gafurov[1]

[1] Institute of Physics, Kazan Federal University,
Kazan, Russia
[2] Ioffe Institute,
St. Petersburg, Russia

E-mail: dev600@mail.ru

Received September 3, 2025
Revised November 8, 2025
Accepted November 8, 2025

The negatively charged boron vacancy in hexagonal boron nitride is one of the most prominent representatives of an optically active qubit in two-dimensional van der Waals materials. In this case, the electron-nuclear interactions of the boron vacancy with the magnetic moments of the hBN lattice atoms are of particular interest. In this paper, we investigated the nuclear quadrupole interactions of the boron vacancy with the remote nuclear spins of nitrogen ^{14}N ($I = 1$) using the method of electron-nuclear double resonance. Comparative analysis of the obtained parameters of the nuclear quadrupole interaction with the parameters for the nitrogen atoms closest to the vacancy is carried out. Based on the data presented, it is proposed to use the electron spin of the boron vacancy as a spin probe to study the fundamental properties of boron nitride, such as the constants of the nuclear quadrupole interaction.

Keywords: electron paramagnetic resonance, ENDOR, boron vacancy, hBN, nuclear quadrupole interaction.

DOI: 10.61011/PSS.2025.11.62965.245-25

1. Introduction

Hexagonal boron nitride (hBN) — Van-der-Waals material with a wide band gap (~ 6 eV) [1,2] — has recently become one of the key objects in the field of quantum technologies [2–6] and two-dimensional nanoelectronics based on Van der Waals heterostructures [2,3,7]. In particular, based on the point defects in hBN the sources of single photons are created for quantum telecommunications [2,3,5,8], quantum sensors of magnetic fields, temperature and pressure [9,10], and also new approaches to optical polarization of nuclear spins [11,12]. Optically active point defects in hBN are of special interest in this context, having the property of polarization of electronic spin states under the action of the optical pumping, first found in hBN in papers [6,8].

Thus, in paper [6] the unambiguous identification of such defect was carried out in the form of a negatively charged vacancy of boron (V_B^-), the structure, spin and optical properties of which are given in Figure 1, *a*. The V_B^- defect has the ground triplet ($S = 1$) state, optically induced inverse population of the spin sublevel $m_s = 0$ at room temperature and, due to the spin-dependent channel of optical recombination from the excited (ES) to the ground (GS) state via a metastable level (MS), the possibility to record the signal of optically detected magnetic resonance (ODMR) via photoluminescence (PL). In paper [8] such unambiguous identification was not conducted; nevertheless, an assumption was made that the point defects related to the admixture of carbon may have optical polarization of electron spins at room temperature, which made it possible for the Authors of the article to demonstrate reading of electron spins of these defects by ODMR. The results of these two papers gave momentum to the explosive development of the studies of optically addressed spin states of point defects in hBN, which caused detection of a wide spectrum of defects having the property of optically induced dominant population of spin sublevels [13–15]. This made it possible to implement high-coherence qubits on their basis [16–18], approach the development of electron-nuclear spin registers [15] by detection and coherent control of a single nuclear spin, related to the defect [15], and also develop some high-sensitivity quantum sensors of subnanometer scale, due to the ability of hBN to be isolated at the monoatomic two-dimensional (2D) level [9,10,18]. It should be noted that the reproducibility of defect formation with the specified type in hBN is of principal importance for the systematic research of their properties, development of device prototypes on their basis, and ensuring stability of their characteristics and the obtained results. Currently specifically for the negatively charged vacancy of boron in hBN it was demonstrated that it was possible to reproduce the defect with the specified properties, which was achieved by radiation of the material with high energy particles (neutrons, electrons, protons and light ions) [6,19–21]. The important feature

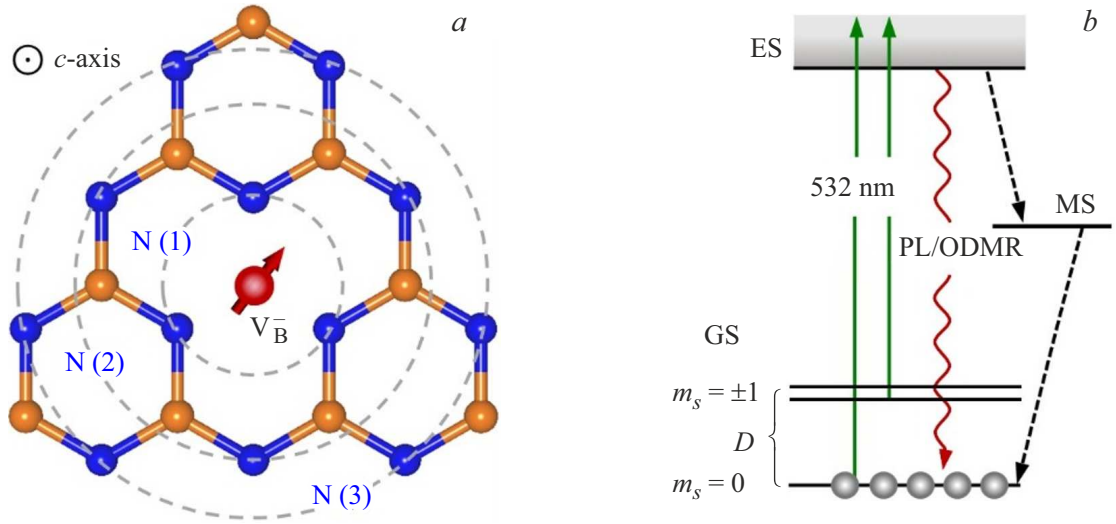

Figure 1. *a*) hBN structure with V_B^- defect (shown in red). Blue shows nitrogen atoms, yellow — boron atoms. The hexagonal axis **c** is directed perpendicularly to the basal 2D−BN-plane (figure plane). Dotted lines show 3 spheres of nitrogen atoms — N(1), N(2), N(3), closest to V_B^-. N(1) and N(2) contain 3 nitrogen atoms each, and N(3) — 6 atoms. *b*) Energy scheme of levels of optical pumping cycle of spin sublevel $m_s = 0$ in GS of V_B^- defect. Spin sublevels of a triplet are split in a zero magnetic field by into value D, shown with a curly bracket. Optical excitation at 532 nm (solid arrows) causes transition of electrons from GS to ES; and then returning to the ground state by optical recombination (PL, red wavy line) without a change in the spin projection. Due to the presence of MS levels in the system, a spin-dependent recombination occurs (indicated with dashed arrows), causing dominant population of $m_s = 0$ and making it possible to read the electron spin of a boron vacancy by ODMR method by change of PL signal intensity at the moment of electron spin resonance.

of hBN is the fact that its lattice is 100 % magnetic nuclei (^{14}N, spin $I = 1$, natural abundance (n.a.) 99.9 %; ^{10}B, $I = 3$, n.a. 19.9 %; ^{11}B, $I = 3/2$, n.a. 80.1 %), with the nuclear spin higher than $I = 1/2$. Therefore, they make an inevitable contribution to the spin Hamiltonian of the boron vacancy not only via hyperfine interactions (HFI), but via nuclear quadrupole interactions (NQI), too. This circumstance results, on the one hand, in considerable losses of coherence of electron spin of the boron vacancy due to the above interactions; on the other hand, to interesting multi-particle quantum effects that are pronounced in the behavior of vacancy spin coherence in small and high magnetic fields with the boundary along the magnetic field in the area of 1 T, as it was theoretically and experimentally shown in papers [22,23]. The important feature of electron-nuclear interactions in such systems is the fact that using the standard methods of electron spin resonance, it becomes impossible to directly receive information on the nuclear quadrupole interactions, since the latter make no contribution to the signal of the electron spin resonance according to the rules of selection of the permitted magnetic dipole transitions ($\Delta m_s = \pm 1$; $\Delta m_I = 0$). Therefore, the studies of electron-nuclear interactions in such high-spin systems require the methods related to the observation of the signals of nuclear magnetic resonance (NMR), with the selection rules ($\Delta m_s = 0$; $\Delta m_I = \pm 1$).

2. Theoretical part

Electron-nuclear double resonance (ENDOR), which makes it possible to record the flips of the nuclear spins via the change in the intensity of the signals of the electron spin resonance in accordance with the selection rules ($\Delta m_s = 0$; $\Delta m_I = \pm 1$), application of an additional saturating radio frequency field leads to resonant transitions with the transitions between the nuclear spin sublevels of atoms bound to the electron spin of the defect via the HFI and NQI. Schematically the structure of energy levels and NMR transitions in the system ($S = 1$; $I = 1$) is shown in Figure 2, according to the spin Hamiltonian (1) describing the center V_B^-:

$$\begin{aligned}\widehat{H} = {} & g\mu_B B_0 S_z + D\left(S_z^2 - \frac{S(S+1)}{3}\right) \\ & + \sum_i \left[A_{zz} S_z I_{zi} + A_{xx} S_x I_{xi} + A_{yy} S_y I_{yi}\right] \\ & + \sum_i \left[g_N \mu_N B_0 I_{zi} + \frac{\chi_q}{4I(2I-1)}\right. \\ & \left. \times \left(3I_{zi}^2 - I(I+1) + \eta(I_{xi}^2 - I_{yi}^2)\right)\right], \end{aligned} \quad (1)$$

where the first two terms describe Zeeman and fine interaction; μ_B — is a Bohr magneton; A_{xx}, A_{yy},

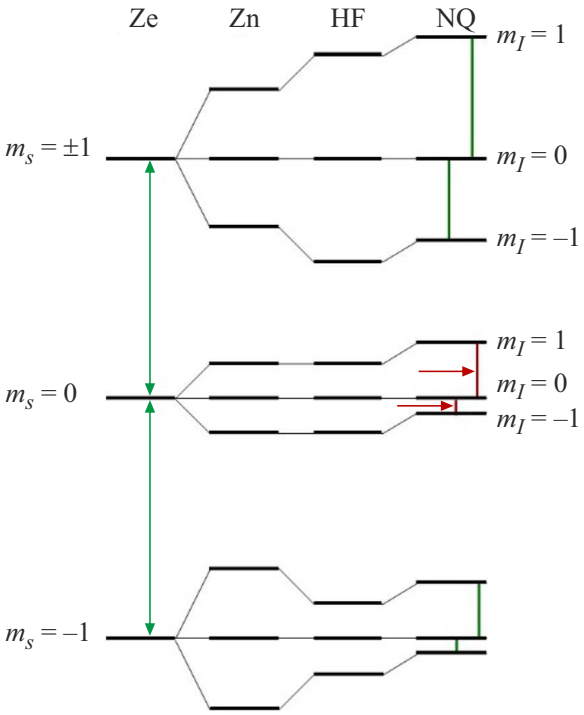

Figure 2. Energy levels of defect V_B^-, interacting with nuclear spins ^{14}N, including electron Zeeman splitting (Ze) and splitting in the zero magnetic field, hyperfine interaction (HF), nuclear quadrupole interaction (NQ) and nuclear Zeeman interaction (Zn). The levels are marked with the corresponding quantum numbers m_s, m_I. The permitted EPR transitions are shown with vertical arrows. The NMR transitions are shown in green (for $m_s = \pm 1$) and dark-red (for $m_s = 0$) lines. The dark-red horizontal arrows specify the NMR transitions caused exclusively by quadrupole interaction with ^{14}N.

A_{zz} — are energies of hyperfine interaction of electron in V_B^- defect and surrounding nuclei, accordingly, reflecting isotropic $(A_{iso} = (A_{xx} + A_{yy} + A_{zz})/3)$ and anisotropic $((2A_{zz} - A_{xx} - A_{yy})/6)$ parts of HFI $\chi_q = eQ_N V_{zz}/h$ — is a nuclear quadrupole constant of splitting that characterizes the interaction of nuclear electric quadrupole moment $(e \cdot Q_N)$ with the electric field gradient in the point of the nucleus (V_{zz}, the main component of the EFG tensor), $\eta = (V_{xx} - V_{yy})/V_{zz}$ — anisotropy of this interaction. Summing by i includes all surrounding nuclei, g_N and μ_N (nuclear g-factor $g_N(^{14}N) = +0.4037$) and nuclear magneton, accordingly. It should be noted that the scheme of the levels specified in Figure 2 is expected in the case when all nuclear magnetic torques are equivalent, which should be expected in the orientation of the induction vector of the external magnetic field directed in parallel to the hexagonal axis of the crystal ($\mathbf{B}_0 \parallel \mathbf{c}$). In this paper we present the results of the study of the interaction between the gradient of the electric field caused by the presence of the boron vacancy in hBN and the quadrupole nuclear magnetic torques of nitrogen atoms located beyond the first coordination sphere of nitrogen atoms indicated in Figure 1, *a* as N(1). To determine the symmetry of NQI and parameters of the corresponding tensor, we studied the NMR transitions (shown in dark-red in Figure 2, *a*) between the nuclear spin sublevels in the state with the projection of the electron spin of boron vacancy $m_s = 0$ by ENDOR method. Such approach makes it possible to directly record exclusively the contribution from the nuclear quadrupole interaction, in virtue of the fact that HFI is absent for the state with the zero projection of the electron spin as you can see it from the spin Hamiltonian (1). At the same time in the ENDOR spectra, according to the scheme of the levels in Figure 2, there must be two pairs of lines from every electronic transition: one pair of lines centered around the Larmor precession frequency of the nuclear magnetic torque ^{14}N,

$$\nu_L = \frac{g_N \mu_N B_0}{h} \approx 10\,\text{MHz}$$

(in high-frequency range at $B_0 \approx 3.3\,\text{T}$), with the distance between them, equal to the value of quadrupole splitting and the second one with the displacement by the HFI value and the same distance between the lines.

Because of different signs m_s for different electronic transitions the displacement will happen in different directions.

3. Experimental part

The paper used commercial single crystals hBN (hq Graphene), radiated with electrons having energy of 2 MeV with dose $6 \cdot 10^{18}\,\text{cm}^{-2}$ to generate defects V_B^- [19]. The experimental studies were carried out using an electron paramagnetic resonance (EPR) spectrometer Bruker Elexsys 680 of high-frequency range (94 GHz) at temperature $T = 25\,\text{K}$. The EPR detected by electron spin echo (ESE) was recorded using standard Hahn pulse sequence ($\pi/2-\tau-\pi-\tau-$ESE) with duration of $\pi/2$-pulse of 48 ns and value of $\tau = 300\,\text{ns}$. To probe nuclear spins, the standard Mims pulse sequence was used ($\pi/2-\tau-\pi/2-\pi_{RF}-\pi/2-\tau-$SSE) [24]. The first two microwave $\pi/2$-pulses induced inversion of populations in electron spin levels; the third $\pi/2$-pulse provides for generation of the stimulated spin echo (SSE) signal. In the interval between the second and the third microwave pulses, a radio frequency pulse π_{RF} was applied, which caused inversion of populations of nuclear spin sublevels and inducted NMR transitions. The NMR frequencies were calculated using software EasySpin [25].

4. Results and discussion

As a result of electron irradiation, boron vacancies were created in hBN crystals in the negative charge state, which is indicated by the EPR spectrum recorded in orientation of the external magnetic field directed in parallel to the hexagonal axis **c** ($\mathbf{B} \parallel \mathbf{c}$) (Figure 3, *a*). Indeed, the signals specified with an arrow in the spectrum are characterized by splitting in the magnetic field ΔB, which corresponds to the

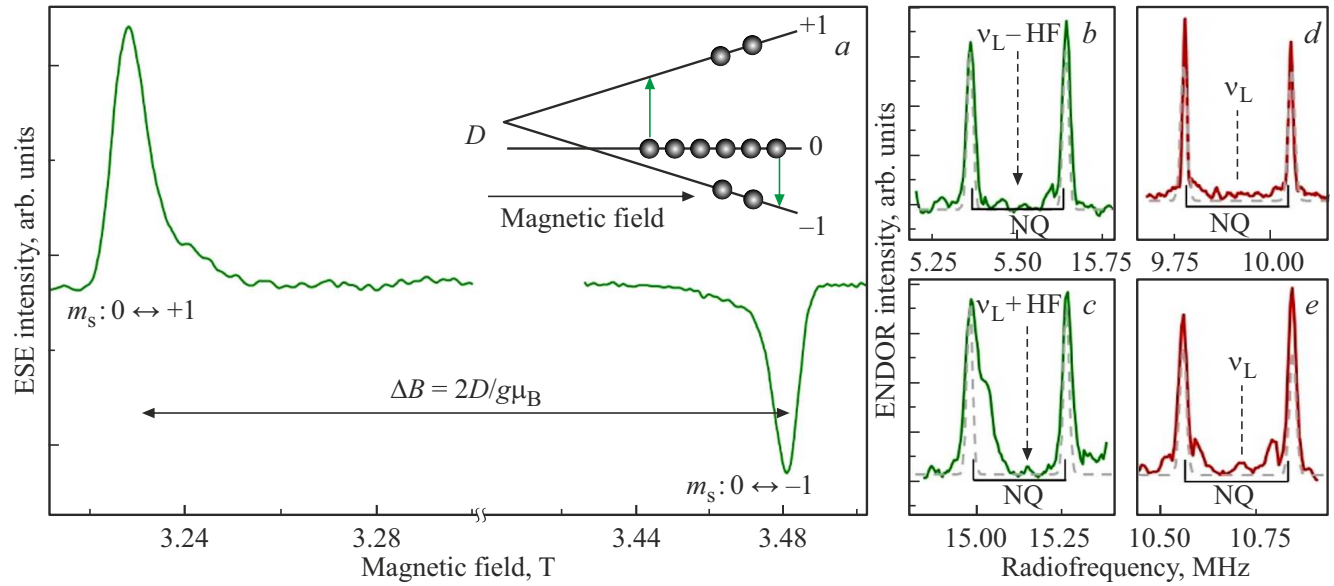

Figure 3. *a*) EPR spectrum of defects V_B^- recorded in the mode of electron spin echo at magnetic field orientation $\mathbf{B} \parallel \mathbf{c}$ and optical pumping with laser $\lambda = 532$ nm. Fine structure transitions between spin sublevels of a triplet with splitting in the magnetic field equal to ΔB (double value of splitting in zero magnetic field, $2D$), are shown with a horizontal arrow. The insert shows schematically the optically induced population of sublevel $m_s = 0$ causing inversion of boron vacancy spin echo signal phases (*b*–*e*). ENDOR spectra are recorded on the components of the fine structure of V_B^- defects. The experimental data is shown in green and dark-red, and the estimated spectra using spin Hamiltonian (*1*) are shown as a grey dotted line. NMR signal frequencies in (*b*) and (*c*) panels comply with NMR transitions between hyperfine sublevels on electron spin sublevels $m_s = +1$ (*b*) and $m_S = -1$ (*c*), and frequencies in (*d*) and (*e*) — between quadrupole split nuclear sublevels to the state with the electron spin projection $m_s = 0$. The position of the Larmor precession frequency ^{14}N, ν_L is shown with a dotted arrow. Splitting between the pairs of the lines on each panel depends on NQI and is marked as NQ. The shift of the quadrupole split lines to the HFI value is marked in (*b*) and (*c*) panels with dotted arrows $\nu_L \pm$ HF.

double value of triplet spin sublevel splitting ($S = 1$) in the zero magnetic field, schematically indicated in the insert in Figure 3, *a* as D. Namely, $\Delta B \cong 255$ mT $\approx 2D/g\mu_B$, where the splitting value in the zero magnetic field $D \approx 3.57$ GHz; g — electron g-factor, $g \approx 2.00$. Parameters D and g correspond to the previously detected methods of microwave spectroscopy [6,19]. The first step to study NQI with the nitrogen nuclei at the distance from the boron vacancy was to record the ENDOR spectra in both components of the thin structure corresponding to transitions m_s: $0 \leftrightarrow +1$ and m_s: $0 \leftrightarrow -1$ and designated in Figure 3, *a*. As expected according to the scheme of levels shown in Figure 2, ENDOR spectra contain eight NMR transitions presented in Figure 3, *b*–*e*. Also note that different electronic transitions are observed with significantly different values of magnetic field induction B_0, the position ν_L varies greatly. From the position of the NMR frequencies at the parallel orientation of the magnetic field you may find the values of HFI and NQI for 4.41 and 0.37 MHz, respectively.

To determine the symmetry and absolute values of the tensor in the NQI center V_B^- with remote atoms ^{14}N, the angular dependence of NMR transitions was studied in the electron spin state $m_s = 0$ in the ENDOR spectra as the induction vector of magnetic field rotated from $\mathbf{B}_0 \parallel \mathbf{c}$ to the orientation $\mathbf{B}_0 \perp \mathbf{c}$, corresponding to the case when the field vector is in plane (0001) of hBN volume crystal.

Under such rotation the magnetic nuclei become non-equivalent, and each nucleus ^{14}N provides two lines in the ENDOR spectrum. Therefore, in case of studies of interactions with nuclear spins in the nitrogen sphere marked as N(2) in Figure 1, we expect to see 6 lines in the NMR spectrum for each sublevel m_s, whereas in the case of interaction with nuclear spins in sphere N(3) we expect to observe a set of 12 NMR lines in the ENDOR spectra. The results of such measurements together with the estimated pathway of the angular dependence of the lines are given in Figure 4. Figure 4, *a* shows the spectra recorded in orientation of the magnetic field $\mathbf{B}_0 \parallel \mathbf{c}$. NMR signals correspond to transitions m_I: $0 \leftrightarrow +1$ and m_I: $0 \leftrightarrow -1$, inducted into state with $m_s = 0$, and correspond to signals shown in Figure 3, *d* and *c*. Dependence of the lines position in the ENDOR spectrum on direction of the magnetic field calculated in EasySpin software is shown in Figure 4, *b*. From the angular dependence you can see how each pair of the lines recorded in orientation $\mathbf{B}_0 \parallel \mathbf{c}$, corresponding to the case when all magnetic torques are equivalent breaks into 12 lines with the angle increase. The progress of the lines in the angular dependence and the spectra recorded in orientation $\mathbf{B}_0 \perp \mathbf{c}$, given in Figure 4, *c*, are described with parameter of quadrupole interaction $\chi_q = 0.37$ MHz and $\eta = 0.55$ MHz. It should be noted that these experimental data for the measurement of NQI

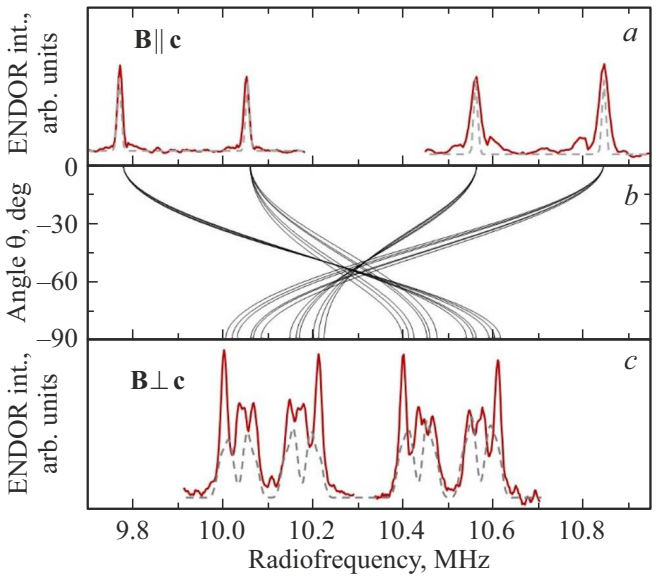

Figure 4. *a*) ENDOR spectra recorded for both components of fine structure of V_B^- defects in orientation of magnetic field $\mathbf{B}_0 \parallel \mathbf{c}$ at sublevel $m_s = 0$. The spectra comply with the ones given in Figure 3, *d* and *e*. Magnetic field values for this orientation: low field component $B_{lf} = 3221.4$ mT and high field $B_{hf} = 3476.5$ mT. *b*) Estimation of angular dependence of the code of the lines in ENDOR spectrum in the rotation of the magnetic field induction vector from parallel to perpendicular orientation relative to axis **c** of the crystal. *c*) ENDOR spectra measured in orientation $\mathbf{B}_0 \perp \mathbf{c}$. Estimation of spectra at $\mathbf{B}_0 \parallel \mathbf{c}$ and $\mathbf{B}_0 \perp \mathbf{c}$ is shown with grey dotted lines. Values of magnetic field for this orientation: $B_{lf} = 3289.8$ mT and $B_{hf} = 3418.8$ mT.

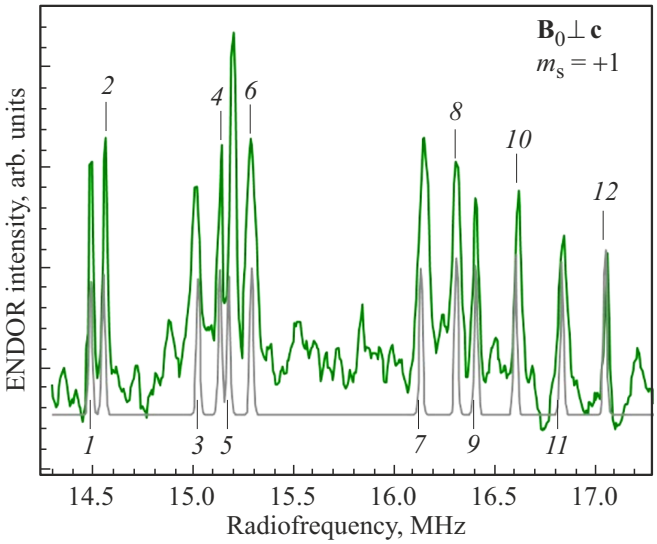

Figure 5. ENDOR spectrum recorded in orientation of magnetic $\mathbf{B}_0 \perp \mathbf{c}$ on a sublevel with electron spin projection $m_s = +1$. A set of 12 NMR transitions is accordingly numbered. Grey is for the estimated ENDOR spectrum obtained using spin Hamiltonian (*1*) and parameters $\chi_q = 0.37$ MHz; $\eta = 0.55$ MHz; $A_{iso} = 5.23 \pm 0.03$ MHz, $A_{dd} = 0.82 \pm 0.03$ MHz. Value of fixed magnetic field for this orientation $B = 3235.8$ mT.

of the center V_B^- using nuclear spin sublevels are in good agreement with the previously measured ENDOR spectra in the states with the HFI impurity, compliant with the projections of the electron spin $m_s = \pm 1$ [26]. The latter is an additional resource to compare and test the values of the directly measured NQI value with nitrogen atoms, which is possible by analysis of the ENDOR spectrum measured using non-zero projection of the electron spin of the boron vacancy. Thus, Figure 5 shows the ENDOR spectrum measured in the state $m_s = +1$ at orientation of the magnetic field $\mathbf{B}_0 \perp \mathbf{c}$. Its theoretical description using spin Hamiltonian (1) with parameters of nuclear quadrupole interaction obtained from the ENDOR description given in Figure 4 of the following hyperfine interaction constants $A_{iso} = 5.23 \pm 0.03$ MHz, $A_{dd} = 0.82 \pm 0.03$ MHz indicates the accuracy of NQI value detection. Additionally note the pronounced structure of the spectrum in Figure 5, which contains 12 lines. This corresponds to 6 non-equivalent atoms of nitrogen in orientation $\mathbf{B}_0 \perp \mathbf{c}$ and unambiguously indicates that the crystalline field gradient was studied in the atoms of the third sphere marked in Figure 1 as N(3).

5. Conclusion

The NQI with the remote nitrogen atoms located in the third coordination sphere of V_B^- defect was studied. A certain value of NQI constant is set as equal to $\chi_q = 0.37$ MHz, which is much lower than the interaction with ^{14}N, located in the first coordination sphere of boron vacancy (N(1) in Figure 1, *a*), specified previously as equal to $\chi_q \approx 1.5$ MHz [27]. This observation reflects the fact that the further from the boron vacancy, the smaller the electron density associated with the defect, contributing minimally to the distortion of the internal electric field of hBN. Therefore, spin density of boron vacancy makes it possible to probe the internal nuclear properties of hBN using the methods of microwave spectroscopy. Thus, previously in order to study the constants of nuclear quadrupole interaction in hBN, they used a single NV-defect in the diamond as the spin probe [28]. Dynamics of its spin coherence recorded using pulse sequence XY8 made it possible to study the parameters of quadrupole interactions in hBN; in particular, it was clearly possible to experimentally find the constant of the quadrupole interaction for internal nuclei of lattice isotope ^{11}B ($\chi_q(^{11}\text{B}) = 2.9221 \pm 0.0006$ MHz). In this context, the V_B^- defect may play a role of its own spin probe in the hBN lattice, which will make it possible to perform alternative and supplemental studies of its spin fundamental properties.

Funding

The study was supported by grant No. 24-12-00151 from the Russian Science Foundation.

Conflict of interest

The Authors declare that they have no conflict of interest.

References

[1] G. Cassabois, P. Valvin, B. Gil. Nature Photon. **10**, *4*, 262 (2016).

[2] J.D. Caldwell, I. Aharonovich, G. Cassabois, J.H. Edgar, B. Gil, D.N. Basov. Nature Rev. Mater. **4**, *8*, 552 (2019).

[3] W. Ren, P. Bøggild, J. Redwing, K. Novoselov, L. Sun, Y. Qi, K. Jia, Z. Liu, O. Burton, J. Alexander-Webber, S. Hofmann, Y. Cao, Y. Long, Q.-H. Yang, D. Li, S.H. Choi, K.K. Kim, Y.H. Lee, M. Li, Q. Huang, Y. Gogotsi, N. Clark, A. Carl, R. Gorbachev, T. Olsen, J. Rosen, K.S. Thygesen, D.K. Efetov, B.S. Jessen, M. Yankowitz, J. Barrier, R.K. Kumar, F.H.L. Koppens, H. Deng, X. Li, S. Dai, D.N. Basov, X. Wang, S. Das, X. Duan, Z. Yu, M. Borsch, A.C. Ferrari, R. Huber, M. Kira, F. Xia, X. Wang, Z.-S. Wu, X. Feng, P. Simon, H.-M. Cheng, B. Liu, Y. Xie, W. Jin, R.R. Nair, Y. Xu, Q. Zhang, A.K. Katiyar, J.-H. Ahn, I. Aharonovich, M.C. Hersam, S. Roche, Q. Hua, G. Shen, T. Ren, H.-B. Zhang, C.M. Koo, N. Koratkar, V. Pellegrini, R.J. Young, B. Qu, M. Lemme, A.J. Pollard. arXiv preprint arXiv:2503.22476 (2025).

[4] Q.H. Wang, A. Bedoya-Pinto, M. Blei, A.H. Dismukes, A. Hamo, S. Jenkins, M. Koperski, Y. Liu, Q.-C. Sun, E.J. Telford, H.H. Kim, M. Augustin, U. Vool, J.-X. Yin, L.H. Li, A. Falin, C.R. Dean, F. Casanova, R.F.L. Evans, M. Chshiev, A. Mishchenko, C. Petrovic, R. He, L. Zhao, A.W. Tsen, B.D. Gerardot, M. Brotons-Gisbert, Z. Guguchia, X. Roy, S. Tongay, Z. Wang, M.Z. Hasan, J. Wrachtrup, A. Yacoby, A. Fert, S. Parkin, K.S. Novoselov, P. Dai, L. Balicas, E.J.G. Santos. ACS Nano **16**, *5*, 6960 (2022).

[5] A. Boretti, J. Blackledge, S. Castelletto. Mater. Sci. Semicond. Process. **185**, 108932 (2025).

[6] A. Gottscholl, M. Kianinia, V. Soltamov, S. Orlinskii, G. Mamin, C. Bradac, C. Kasper, K. Krambrock, A. Sperlich, M. Toth, I. Aharonovich, V. Dyakonov. Nature Mater. **19**, *5*, 540 (2020).

[7] K.S. Novoselov, A. Mishchenko, A. Carvalho, A.H. Castro Neto. Sci. **353**, *6298*, aac9439 (2016).

[8] N. Chejanovsky, A. Mukherjee, J. Geng, Y.-C. Chen, Y. Kim, A. Denisenko, A. Finkler, T. Taniguchi, K. Watanabe, D.B.R. Dasari, P. Auburger, A. Gali, J.H. Smet, J. Wrachtrup. Nature Mater. **20**, *8*, 1079 (2021).

[9] A. Gottscholl, M. Diez, V. Soltamov, C. Kasper, D. Krauße, A. Sperlich, M. Kianinia, C. Bradac, I. Aharonovich, V. Dyakonov. Nature Commun. **12**, *1*, 4480 (2021).

[10] S. Vaidya, X. Gao, S. Dikshit, I. Aharonovich, T. Li. Adv. Phys.: X, **8**, *1*, 2206049 (2023).

[11] F.T. Tabesh, M. Fani, J.S. Pedernales, M.B. Plenio, M. Abdi. Phys. Rev. B **107**, *21*, 214307 (2023).

[12] X. Gao, S. Vaidya, K. Li, P. Ju, B. Jiang, Z. Xu, A.E. Llacsahuanga Allcca, K. Shen, T. Taniguchi, K. Watanabe, S.A. Bhave, Y.P. Chen, Y. Ping, T. Li. Nature Mater. **21**, *9*, 1024 (2022).

[13] N. Mendelson, D. Chugh, J.R. Reimers, T.S. Cheng, A. Gottscholl, H. Long, C.J. Mellor, A. Zettl, V. Dyakonov, P.H. Beton, S.V. Novikov, C. Jagadish, H.H. Tan, M.J. Ford, M. Toth, C. Bradac, I. Aharonovich. Nature Mater. **20**, *3*, 321 (2021).

[14] H.L. Stern, C.M. Gilardoni, Q. Gu, S.E. Barker, O.F.J. Powell, X. Deng, S.A. Fraser, L. Follet, C. Li, A.J. Ramsay, H.H. Tan, I. Aharonovich, M. Atatüre. Nature Mater. **23**, *10*, 1379 (2024).

[15] X. Gao, S. Vaidya, K. Li, Z. Ge, S. Dikshit, S. Zhang, P. Ju, K. Shen, Y. Jin, Y. Ping, T. Li. Nature **643**, *8073*, 943 (2025).

[16] R. Rizzato, M. Schalk, S. Mohr, J.C. Hermann, J.P. Leibold, F. Bruckmaier, G. Salvitti, C. Qian, P. Ji, G.V. Astakhov, U. Kentsch, M. Helm, A.V. Stier, J.J. Finley, D.B. Bucher. Nature Commun. **14**, *1*, 5089 (2023).

[17] A. Haykal, R. Tanos, N. Minotto, A. Durand, F. Fabre, J. Li, J.H. Edgar, V. Ivady, A. Gali, T. Michel, A. Dréau, B. Gil, G. Cassabois, V. Jacques. Nature Commun. **13**, *1*, 4347 (2022).

[18] C.M. Gilardoni, S.E. Barker, C.L. Curtin, S.A. Fraser, O.F.J. Powell, D.K. Lewis, X. Deng, A.J. Ramsay, S. Adhikari, C. Li, I. Aharonovich, H.H. Tan, M. Atatüre, H.L. Stern. Nature Commun. **16**, *1*, 4947 (2025).

[19] F.F. Murzakhanov, B.V. Yavkin, G.V. Mamin, S.B. Orlinskii, I.E. Mumdzhi, I.N. Gracheva, B.F. Gabbasov, A.N. Smirnov, V.Y. Davydov, V.A. Soltamov. Nanomater. **11**, *6*, 1373 (2021).

[20] F.F. Murzakhanov, I.E. Mumdzhi, G.V. Mamin, R.V. Yusupov, V.Yu. Davydov, A.N. Smirnov, M.V. Muzafarova, S.S. Nagalyuk, V.A. Soltamov. Phys. Solid State **64**, *4*, 210 (2022).

[21] M. Hennessey, B. Whitefield, A. Gale, M. Kianinia, J.A. Scott, I. Aharonovich, M. Toth. Adv. Quantum Technol. **8**, *2*, 2300459 (2025).

[22] A. Tárkányi, V. Ivády. arXiv:2505.03292 (2025).

[23] J. Lee, H. Kim, H. Park, H. Seo. arXiv:2505.03306 (2025).

[24] W.B. Mims. Proc. R. Soc. London, Ser. A **283**, *1395*, 452 (1965).

[25] S. Stoll, A. Schweiger. J. Magn. Reson. **178**, *1*, 42 (2006).

[26] G.V. Mamin, E.V. Dmitrieva, F.F. Murzakhanov, I.N. Gracheva, E.N. Mokhov, I.I. Vlasov, M.R. Gafurov, U. Gerstmann, V.A. Soltamov. Appl. Phys. Lett. **127**, *2*, 024001 (2025).

[27] F.F. Murzakhanov, G.V. Mamin, S.B. Orlinskii, U. Gerstmann, W.G. Schmidt, T. Biktagirov, I. Aharonovich, A. Gottscholl, A. Sperlich, V. Dyakonov, V.A. Soltamov. Nano Lett. **22**, *7*, 2718 (2022).

[28] I. Lovchinsky, J.D. Sanchez-Yamagishi, E.K. Urbach, S. Choi, S. Fang, T.I. Andersen, K. Watanabe, T. Taniguchi, A. Bylinskii, E. Kaxiras, P. Kim, H. Park, M.D. Lukin. Sci. **355**, *6324*, 503 (2017).

Translated by M.Verenikina